Nonlinear viscoelastic characterization of bovine trabecular bone

Biomechanics and Modeling in Mechanobiology manuscript No.
(will be inserted by the editor)

Nonlinear viscoelastic characterization of bovine trabecular bone

Krishnagoud Manda · Robert J. Wallace · Shuqiao Xie · Francesc Levrero-Florencio · Pankaj Pankaj

the date of receipt and acceptance should be inserted later

Abstract The time-independent elastic properties of trabecular bone have been extensively investigated and several stiffness-density relations have been proposed. Although it is recognised that trabecular bone exhibits time-dependent mechanical behaviour, a property of viscoelastic materials, the characterization of this behaviour has received limited attention. The objective of the present study was to investigate the time-dependent behaviour of bovine trabecular bone through a series of compressive creep-recovery experiments and to identify its nonlinear constitutive viscoelastic material parameters. Uniaxial compressive creep and recovery experiments at multiple loads were performed on cylindrical bovine trabecular bone samples (n = 19). Creep response was found to be significant and always comprised of recoverable and irrecoverable strains, even at low stress/strain levels. This response was also found to vary nonlinearly with applied stress. A systematic methodology was developed

Krishnagoud Manda (✉) · Shuqiao Xie · Francesc Levrero-Florencio · Pankaj Pankaj

School of Engineering, The University of Edinburgh, The King's Buildings, Edinburgh, EH9 3DW, UK

E-mail: k.manda@ed.ac.uk

Robert J. Wallace

Department of Orthopaedics, The University of Edinburgh, Chancellors building, Edinburgh, EH16 4SB, UK

to separate recoverable (nonlinear viscoelastic) and irrecoverable (permanent) strains from the total experimental strain response. We found that Schapery's nonlinear viscoelastic constitutive model describes the viscoelastic response of the trabecular bone, and parameters associated with this model were estimated from the multiple load creep-recovery (MLCR) experiments. Nonlinear viscoelastic recovery compliance was found to have a decreasing and then increasing trend with increasing stress level, indicating possible stiffening and softening behaviour of trabecular bone due to creep. The obtained parameters from MLCR tests, expressed as second order polynomial functions of stress, showed a similar trend for all the samples, and also demonstrate stiffening-softening behaviour with increasing stress.

Keywords Creep · recovery · nonlinear viscoelasticity · recoverable and irrecoverable strains · trabecular bone · Schapery model

1 Introduction

Trabecular bone is an open porous composite cellular solid material from an engineering perspective. The apparent level mechanical properties of this cellular material depend on its heterogeneous microstructure, which varies with age, disease, gender and anatomical site being considered (Keaveny et al, 2001). Bone is known to become more porous with age and due to diseases such as osteoporosis (Rachner et al, 2011). Trabecular bone is anisotropic and principal trabecular orientations vary with anatomical site; it is also recognised that its anisotropic character becomes pronounced with age (Singh et al, 1970). The density of this cellular solid has been related to its time-independent elastic stiffness in a number of studies (Currey, 1986; Morgan et al, 2003) and these relations are frequently used in computational models of bone and bone-implant systems (Goffin et al, 2013). It has also been recognised that the response of bone to mechanical loads is, in reality, time-dependent (Schoenfeld et al,

1974; Zilch et al, 1980). The study of time-dependent behaviour is of interest in a number of contexts: loosening of orthopaedic implants; non traumatic fractures due to prolonged load over time; viscoelastic compatibility of synthetic bone substitutes; and energy absorption during dynamic loads (Norman et al, 2006; Pollintine et al, 2009; Phillips et al, 2006; Linde et al, 1989).

The time-dependent mechanical behaviour of the trabecular bone has been experimentally investigated via relaxation tests (Schoenfeld et al, 1974; Zilch et al, 1980; Deligianni et al, 1994; Bredbenner and Davy, 2006; Quaglini et al, 2009), creep tests (Bowman et al, 1994, 1998; Yamamoto et al, 2006; Manda et al, 2016), and dynamic mechanical tests (Guedes et al, 2006; Kim et al, 2012, 2013). Yamamoto et al (2006) reported that substantial amount of creep develops in the trabecular bone even at smaller load levels corresponding to physiological activities. It has also been found that the time-dependent response is not linear and varies with the applied stress/strain levels (Bowman et al, 1998; Yamamoto et al, 2006; Quaglini et al, 2009), i.e. it cannot be modelled using linear viscoelasticity. However, none of the above studies quantified the nonlinearity in the time-dependent response of the trabecular bone. Characterizing this nonlinearity in the time-dependent behaviour at apparent level is important from both clinical and engineering perspectives. Such characterization can provide: insights into the mechanisms contributing to the creep behaviour of the trabecular bone; improve predictions from finite element modelling of bone and bone-implant systems; and help understand osteoporotic fractures.

Many constitutive equations have been developed for characterizing the nonlinear viscoelastic materials, from single integral (Knauss and Emri, 1981; Schapery, 1969; Christensen, 1980) to multiple integral formulations, see e.g. Findley et al (1976). The single integral representations have been the most widely applied theories for different viscoelastic materials and are relatively easy to implement in a numerical scheme. Previous studies have

developed methodologies to determine the nonlinear viscoelastic parameters based on single integral formulations for materials with power law time dependence (Lou and Schapery, 1971) and with Prony series time-dependence (Nordin and Varna, 2005; Huang et al, 2011). Both creep data during plateau loading and strain recovery data after unloading in a creep-revovery test at different load levels are required for this analysis. Most of these formulations have been used for materials like asphalt concrete and polymers, and the samples were permitted to fully recover between creep-recovery tests at different load levels. However, it is not known how long trabecular bone takes to recover fully between the tests (Yamamoto et al, 2006; Kim et al, 2012; Pollintine et al, 2009). Therefore it is necessary to develop a methodology that takes into account any residual strains and permits continuous application of loading and unloading phases at different load levels without the need for resting the sample between the loading cycles.

Therefore, the primary objectives of the study were three-fold. First, to experimentally measure the time-dependent behaviour of trabecular bone through uniaxial compressive multiple load creep-recovery (MLCR) experiments. Second, to develop a systemic methodology to estimate the associated material parameters from the MLCR tests. Third, to quantify the nonlinearity associated with varying stress levels using the obtained parameters.

2 Materials and methods

2.1 Sample preparation and μCT imaging

Fresh proximal bovine femora, female, under 30 months old when killed, were obtained from a local abattoir and were stored at -20 °C until utilized. The bones were allowed to thaw to room temperature before the femoral heads and trochanters were removed using a hacksaw. Transmission radiographs were then taken to identify the principal direction of

trabeculae, and 19 cores (15 from three femoral heads and 4 from two trochanters) were extracted using a diamond core drill bit (Starlite, Rosemont, USA) and marrow was kept intact in all the samples to mimic the realistic situation of bone as closely as possible. The heads and trochanters were kept hydrated while drilling in a custom made holding clamp to mitigate temperature damage. Once extracted, the cores were examined for the presence of a growth plate, and if found this was removed during sample preparation. A low speed rotating saw (Buehler, Germany) was used to create parallel sections. The cylindrical bone samples in total $n = 19$ were of diameter 10.6 ± 0.1 mm and mean height of 25.0 ± 2.7 mm. Brass end-caps were glued to each end of the sample using bone cement (Simplex, Stryker, UK) to minimize end-artefacts during compression testing (Keaveny et al, 1997). Effective length (22.1 ± 2.6 mm) of each specimen was calculated as the length of the sample between the end-caps plus half the length of the sample embedded within the end-caps (Keaveny et al, 1997), and this effective length was used in calculating average strains.

Before mechanical testing high resolution microcomputed tomography (μCT) scans were taken of each sample using a Skyscan 1172 μCT scanner (Bruker microCT, Kontich, Belgium). The following scan parameters were used: voxel resolution 17.22 μm, source voltage 100 kV, current 100 μA, exposure 1771 ms with a 0.5 mm aluminium filter between the x-ray source and the specimen. Image quality was improved by using 2 frame averaging. The images were reconstructed with no further reduction in resolution using Skyscan proprietary software, nRecon V1.6.9.4 (Bruker microCT, Kontich, Belgium). Morphometric analysis was performed using CTAn software (Bruker microCT, Kontich, Belgium), and by considering the whole volume within each sample the ratio of bone volume to total volume (BV/TV) was evaluated along with other microarchitectural indices: trabecular thickness (Tb.Th), trabecular number (Tb.N), trabecular separation (Tb.Sp) and structure model index (SMI). Homogeneity analysis was performed on each sample by evaluating the above

microarchitectural indices in sub-volumes of four $5 \times 5 \times 5$ mm cubes along the length of each sample. Intra-specimen variations of these indices across each sample were found to be less than $\pm 4\%$ with respect to the values when whole volume was considered indicating fairly homogeneous nature and uniform bone quality of each sample. A water bath filled with phosphate-buffered saline (PBS) was used around each sample to keep it hydrated at all times during imaging and through all phases of mechanical testing.

2.2 Creep-recovery experiments

Following μCT scanning, each sample was preconditioned by applying 0.1% apparent strain for ten cycles (Bowman et al, 1994) and was then allowed to recover for 30 minutes prior to the main mechanical testing. The compressive multiple load creep-recovery (MLCR) experiments as shown in Fig. 1 were conducted on 19 trabecular bone samples using Zwick material testing machine (Zwick Roell, Herefordshire, UK). The trabecular bone macroscopically yields below 0.8% strains in compression (Kopperdahl and Keaveny, 1998; Morgan et al, 2001) in an isotropic manner in strain space (Levrero-Florencio et al, 2016). Therefore, we chose the static strains of 0.2%, 0.4%, 0.6%, 0.8%, 1.0%, 1.5%, 2.0% and 2.5% in cycles I-VIII, respectively, to measure the time-dependent behaviour at pre and post yield regime. These target strains were specified to the Zwick machine in the MLCR tests on each sample which in turn applied the force as a ramp at a strain rate of 0.01 s^{-1}, and when the targeted static strain was reached, a constant load corresponding to this strain was automatically maintained by the machine for 200 s. Each loading step was followed by an unloading step (again at a strain rate of 0.01 s^{-1}) to almost zero (2 N) force, which was maintained for 600 s (see upper part of Fig. 1). This small load of 2 N was to ensure that end-caps remained in contact with the load applicator. The creep deformation was recorded during the loading

phase of 200 s and also during the strain recovery (unloading phase) of 600 s for each cycle throughout the experiment for each sample (lower part of Fig. 1). All the tests were load controlled. In our pilot studies, we observed that the creep rate (slope of the creep vs time curve) becomes constant in less than 200 s during the loading phase (at load levels of interest). Similarly in the recovery phase the recovery curves were found to reach a plateau in less than 600 s. Hence, we chose the creep time as 200 s and recovery time as 600 s for all samples in all cycles.

These multiple plateau loads corresponding to above mentioned static strains were converted to stresses by dividing them with cross sectional area of each sample. The experiments were stopped if the tertiary creep or failure occurred during the loading phase at any stress level. The tertiary creep or failure was defined as response where creep strain accelerates rapidly and increases beyond 5.0%. In the following sections we use the term 'load' in Newtons and 'stress' in MPa interchangeably, and also a term 'applied static strain' which indicates the plateau loads/stresses corresponding to static strains of 0.2%, 0.4%, 0.6%, 0.8%, 1.0%, 1.5%, 2.0% and 2.5% in the loading cycles I, II, III, IV, V, VI, VII and VIII, respectively.

2.3 Material model

The time-dependent strain response ($\varepsilon_{tot}(t)$) of trabecular bone to an applied load is given by

$$\varepsilon_{tot}(t) = \varepsilon_{nve}(t) + \varepsilon_{irrec}(t) \tag{1}$$

where $\varepsilon_{irrec}(t)$ is the irrecoverable strain response and $\varepsilon_{nve}(t)$ is the recoverable nonlinear viscoelastic strain. For linear viscoelastic materials $\varepsilon_{nve}(t) = \varepsilon_{ve}(t)$ and Boltzmann superposition integral, can be used to represent the stress-strain relations (Findley et al, 1976), is

given by

$$\varepsilon_{ve}(t) = \int_0^t D(t-\tau)\frac{d\sigma}{d\tau}\tau \tag{2}$$

or, equivalently

$$\varepsilon_{ve}(t) = D_0\sigma + \int_0^t \Delta D(t-\tau)\frac{d\sigma}{d\tau}\tau \tag{3}$$

where σ is an arbitrary stress input, $D(t) = D_0 + \Delta D(t)$ is the total creep compliance, D_0 is instantaneous compliance that describes the elastic response at time $t = 0$ and $\Delta D(t)$ is the transient creep compliance that evolves with time. In an ideal creep-recovery test, the plateau stress σ is applied at time $t = 0$ and removed at $t = t_a$ (see the first cycle in Fig. 1). By substituting this step input of stress σ into Eq. 3, the resulting creep strain response (ε_{cr}) during loading phase, $0 < t < t_a$, in a typical creep-recovery test is obtained as

$$\varepsilon_{cr}(t) = D_0\sigma + \Delta D(t)\,\sigma + \varepsilon_{irrec}(t) \tag{4}$$

and the strain response during recovery period (ε_{re}), $t > t_a$, is given by

$$\begin{aligned}\varepsilon_{re}(t) &= \varepsilon_{cr}(t) - \varepsilon_{cr}(t-t_a)\\ &= [\Delta D(t) - \Delta D(t-t_a)]\,\sigma + \varepsilon_{irrec}(t_a)\end{aligned} \tag{5}$$

It is important to note that it is not possible to perform, in practice, ideal creep-recovery experiments with instantaneous load application at $t = 0$. In this study, the load application in MLCR tests was a finite ramp with the strain rate of 0.01 s^{-1}. We assumed that this strain rate is sufficiently fast to be treated as instantaneous for the range of strains considered in this study; it was, therefore, assumed that it has negligible influence on the results.

Our preliminary experimental analysis revealed that the recoverable behaviour is not linear and is dependent on the applied stress. Also previous studies (Yamamoto et al, 2006; Quaglini et al, 2009) have recognised that the time-dependent behaviour of the trabecular bone is not linear and varies with the applied stress/strain. In order to capture this nonlinearity, the stress-dependent nonlinear viscoelastic models were considered in this study.

Several general constitutive models have been proposed to describe the behaviour of nonlinear viscoelastic materials (Schapery, 1969; Christensen, 1980; Knauss and Emri, 1981). The thermodynamics based theory using single integral nonlinear viscoelasticity developed by Schapery (1969, 1997), which utilizes the same structure as the linear integral model, has been shown to be a convenient formulation (Smart and Williams, 1972). Also, Dillard et al (1987) compared the Schapery's model to several other nonlinear viscoelastic formulations and showed that Schapery's model produces most accurate results for both given stress or strain inputs. It has also been shown that this model is adaptable to many other nonlinear viscoelastic materials, like asphalt concrete (Huang et al, 2011), polymers (Lai and Bakker, 1995), and ligaments (Provenzano et al, 2002). It was, therefore thought to be appropriate for modelling trabecular bone in this study. The nonlinear constitutive parameters in the Schapery's model conveniently describe the nonlinearities based on stress.

The nonlinear viscoelastic model proposed by Schapery (1969) is given by

$$\varepsilon_{nve}(t) = g_0 D_0 \sigma + g_1 \int_0^t \Delta D\left(\psi^t - \psi^\tau\right) \frac{d\left(g_2\sigma\right)}{d\tau} d\tau \tag{6}$$

where g_0, g_1, g_2 and a_σ are stress dependent nonlinear viscoelastic (VE) parameters. The parameter g_0 is a nonlinear instantaneous compliance parameter that scales the reduction or increase in instantaneous elastic compliance. Transient nonlinear parameter g_1 measures the nonlinearity effect in the transient compliance, and the parameter g_2 describes the effect of the loading rate on the transient creep response as well, and ψ^t, called, reduced time, is given by

$$\psi^t = \int_0^t \frac{d\tau'}{a_{\sigma(\tau')} a_{T(\tau')} a_{e(\tau')}} \tag{7}$$

where a_σ, a_T and a_e are stress, temperature and other environment time-shift factors, respectively. In this work, the effects of temperature and other environment variables are not considered and therefore $a_T = a_e = 1$. For the linear viscoelastic materials, the parameters

$g_0 = g_1 = g_2 = a_\sigma = 1$, such that the Eq. 6 reduces to the Boltzmann superposition integral of Eq. 3. The transient compliance in Eq. 6 is represented by Prony series as

$$\Delta D\left(\psi^t\right) = \sum_{n=1}^{N_{pr}} D_n \left[1 - \exp\left(-\lambda_n \psi^t\right)\right] \tag{8}$$

where N_{pr} is number of Prony series parameters, D_n is nth coefficient of the Prony series associated with the reciprocal of nth retardation time, λ_n. Similar to the Eqs. 4 and 5, the strain responses during loading and recovery phases in a typical creep-recovery test are given by

$$\varepsilon_{cr}(t) = g_0 D_0 \sigma + g_1 g_2 \Delta D\left(\frac{t}{a_\sigma}\right)\sigma + \varepsilon_{irrec}(t) \tag{9}$$

and

$$\varepsilon_{re}(t) = \left[g_2 \sigma \Delta D\left(\tfrac{t}{a_\sigma}\right) - g_2 \sigma \Delta D\left(\tfrac{t-t_a}{a_\sigma}\right)\right] + \varepsilon_{irrec}(t_a) \tag{10}$$

and the reduced time in Eq. 7 becomes $\psi^t = t/a_\sigma$.

2.4 Evaluation of model parameters

After selecting Schapery's constitutive theory, the numerical values of its associated parameters were obtained in a systematic manner from the MLCR experimental data. Most of the approaches that have been suggested previously (Lai and Bakker, 1995; Huang et al, 2011) relied on independent creep-recovery tests in which the samples were allowed to recover fully between the tests at different load levels. In this study the experiments were performed continuously at multiple stress levels with loading and unloading phases. Consequently our methodology was required to account for residual strains from the previous loading cycles when evaluating the response of the following loading cycle. A schematic depiction of creep and recovery curves, during loading and unloading phases respectively, at multiple stress levels is shown in Fig. 1.

The components of total strain during the loading and the recovery phases in the first cycle are given by

$$\varepsilon_{cr}^{I}(t) = \left[g_0^I D_0 \sigma^I + g_1^I g_2^I \sigma^I \Delta D\left(\frac{t}{a_\sigma^I}\right)\right] + \varepsilon_{irrec}^{I}(t) \tag{11}$$

and

$$\varepsilon_{re}^{I}(t) = \left[g_2^I \sigma^I \Delta D\left(\frac{t}{a_\sigma^I}\right) - g_2^I \sigma^I \Delta D\left(\frac{t-t_a}{a_\sigma^I}\right)\right] + \varepsilon_{irrec}^{I}(t_a) \tag{12}$$

where superscripts denote the loading cycle number, and subscripts to the time variable t are different time points in the MLCR test as shown in Fig. 1.

First step in the analysis procedure is to obtain the Prony series coefficients associated with linear viscoelastic response. It was assumed that the trabecular bone behaves in a linear viscoelastic manner until the first loading cycle (or at a lowest stress level corresponding to 0.2% of static strain) for each sample. Hence, the corresponding nonlinear VE parameters $g_0^I = g_1^I = g_2^I = a_\sigma^I = 1$ for the first loading cycle. The irrecoverable strain, in the first cycle, is constant once the load is removed at $t = t_a$, and therefore, by taking the difference between Eq. 11 at $t = t_a$ and Eq. 12 it is possible to eliminate the irrecoverable strain and the remainder gives purely recoverable (viscoelastic) response. Therefore, the viscoelastic recovery strain $\Delta\varepsilon_{re1}^{I}$ between t_a and t_b in the first loading cycle is given by

$$\begin{aligned}
\Delta\varepsilon_{re1}^{I}(t) &= \varepsilon_{cr}^{I}(t_a) - \varepsilon_{re}^{I}(t) \\
&= g_0^I D_0 \sigma^I \\
&\quad + \left\{ \begin{array}{l}
g_1^I g_2^I \sigma^I \sum_{n=1}^{N_{pr}} D_n \left[1 - \exp(-\lambda_n \frac{t_a}{a_\sigma^I})\right] \\
-g_2^I \sigma^I \sum_{n=1}^{N_{pr}} D_n \left[1 - \exp\left(-\lambda_n \frac{t}{a_\sigma^I}\right)\right] \\
+g_2^I \sigma^I \sum_{n=1}^{N_{pr}} D_n \left[1 - \exp\left(-\lambda_n \frac{t-t_a}{a_\sigma^I}\right)\right]
\end{array} \right\}
\end{aligned} \tag{13}$$

The unknown linear viscoelastic coefficients D_0, D_n and λ_n ($n = 1, 2, ..., N_{pr}$) were obtained from the first creep-recovery cycle by minimizing the error between the experimental measurements and Eq. 13 using nonlinear least squares fit for each sample. The number of Prony

terms, $N_{pr} = 3$, was found to be sufficient to accurately represent the experimental viscoelastic strain response for all the samples. Also, the viscoelastic recovery compliance in the first cycle was obtained by dividing the $\Delta\varepsilon^{I}_{re1}$ with σ^{I}.

The total strain components for the second loading cycle, during creep and recovery phases, were obtained as

$$\begin{aligned}\varepsilon^{II}_{cr}(t) = {} & g^{II}_0 D_0 \sigma^{II} \\ & + g^{II}_1 \left\{ \begin{array}{l} g^{I}_2 \sigma^{I} \Delta D\left(\frac{t}{a^{I}_{\sigma}}\right) - g^{I}_2 \sigma^{I} \Delta D\left(\frac{t-t_a}{a^{I}_{\sigma}}\right) \\ + g^{II}_2 \sigma^{II} \Delta D\left(\frac{t-t_b}{a^{II}_{\sigma}}\right) \end{array} \right\} \\ & + \varepsilon^{II}_{irrec}(t)\end{aligned} \tag{14}$$

$$\begin{aligned}\varepsilon^{II}_{re}(t) = {} & \left\{ \begin{array}{l} g^{I}_2 \sigma^{I} \Delta D\left(\frac{t}{a^{I}_{\sigma}}\right) - g^{I}_2 \sigma^{I} \Delta D\left(\frac{t-t_a}{a^{I}_{\sigma}}\right) \\ + g^{II}_2 \sigma^{II} \Delta D\left(\frac{t-t_b}{a^{II}_{\sigma}}\right) - g^{II}_2 \sigma^{II} \Delta D\left(\frac{t-t_c}{a^{II}_{\sigma}}\right) \end{array} \right\} \\ & + \varepsilon^{II}_{irrec}(t_c)\end{aligned} \tag{15}$$

Using the previously known Prony coefficients, the unknown nonlinear VE parameters for second cycle need to be evaluated. In order to achieve this, the irrecoverable strain $\varepsilon^{irrec}(t)$ at $t = t_c$ in the second cycle needs to be eliminated by manipulating Eq. 14 and 15. By subtracting the total strain during recovery period $\varepsilon^{II}_{re}(t)$ from itself at time $t = t_2$, the resulting

equation $\Delta\varepsilon^{II}_{re2}(t)$, $t_2 < t < t_d$ contains only two unknown parameters g^{II}_2 and a^{II}_σ as follows

$$\begin{aligned}\Delta\varepsilon^{II}_{re2}(t) &= \varepsilon^{II}_{re}(t_2) - \varepsilon^{II}_{re}(t)\\ &= g^I_2\sigma^I \left\{ \begin{array}{l} \sum_{n=1}^{N_{pr}} D_n \left[1-\exp\left(-\lambda_n \frac{t_2}{a^I_\sigma}\right)\right] \\ -\sum_{n=1}^{N_{pr}} D_n \left[1-\exp\left(-\lambda_n \frac{t_2-t_a}{a^I_\sigma}\right)\right] \\ -\sum_{n=1}^{N_{pr}} D_n \left[1-\exp\left(-\lambda_n \frac{t}{a^I_\sigma}\right)\right] \\ +\sum_{n=1}^{N_{pr}} D_n \left[1-\exp\left(-\lambda_n \frac{t-t_a}{a^I_\sigma}\right)\right] \end{array} \right\}\\ &+g^{II}_2\sigma^{II} \left\{ \begin{array}{l} \sum_{n=1}^{N_{pr}} D_n \left[1-\exp(-\lambda_n \frac{t_2-t_b}{a^{II}_\sigma})\right] \\ -\sum_{n=1}^{N_{pr}} D_n \left[1-\exp\left(-\lambda_n \frac{t_2-t_c}{a^{II}_\sigma}\right)\right] \\ -\sum_{n=1}^{N_{pr}} D_n \left[1-\exp\left(-\lambda_n \frac{t-t_b}{a^{II}_\sigma}\right)\right] \\ +\sum_{n=1}^{N_{pr}} D_n \left[1-\exp\left(-\lambda_n \frac{t-t_c}{a^{II}_\sigma}\right)\right] \end{array} \right\}\end{aligned} \tag{16}$$

These parameters g^{II}_2 and a^{II}_σ were obtained by minimizing the error between measurements of $\Delta\varepsilon^{II}_{re2}$ as shown in Fig. 1 and Eq. 16 using nonlinear least squares method. By taking the difference between the creep strain $\varepsilon^{II}_{cr}(t_c)$ at $t = t_c$ and the strain during recovery period $\varepsilon^{II}_{re}(t)$ at time t in the second cycle, the term $\Delta\varepsilon^{II}_{re1}$ can be obtained as

$$\begin{aligned}\Delta\varepsilon^{II}_{re1}(t) &= \varepsilon^{II}_{cr}(t_c) - \varepsilon^{II}_{re}(t)\\ &= g^{II}_0 D_0 \sigma^{II}\\ &+g^{II}_1 \left\{ \begin{array}{l} g^I_2\sigma^I \sum_{n=1}^{N_{pr}} D_n \left[1-\exp\left(-\lambda_n \frac{t_c}{a^I_\sigma}\right)\right] \\ -g^I_2\sigma^I \sum_{n=1}^{N_{pr}} D_n \left[1-\exp\left(-\lambda_n \frac{t_c-t_a}{a^I_\sigma}\right)\right] \\ +g^{II}_2\sigma^{II} \sum_{n=1}^{N_{pr}} D_n \left[1-\exp\left(-\lambda_n \frac{t_c-t_b}{a^{II}_\sigma}\right)\right] \end{array} \right\}\\ &- \left\{ \begin{array}{l} g^I_2\sigma^I \sum_{n=1}^{N_{pr}} D_n \left[1-\exp\left(-\lambda_n \frac{t}{a^I_\sigma}\right)\right] \\ -g^I_2\sigma^I \sum_{n=1}^{N_{pr}} D_n \left[1-\exp\left(-\lambda_n \frac{t-t_a}{a^I_\sigma}\right)\right] \\ +g^{II}_2\sigma^{II} \sum_{n=1}^{N_{pr}} D_n \left[1-\exp\left(-\lambda_n \frac{t-t_b}{a^{II}_\sigma}\right)\right] \\ -g^{II}_2\sigma^{II} \sum_{n=1}^{N_{pr}} D_n \left[1-\exp\left(-\lambda_n \frac{t-t_c}{a^{II}_\sigma}\right)\right] \end{array} \right\}\end{aligned} \tag{17}$$

The remaining two parameters g^{II}_0 and g^{II}_1 were obtained by minimizing the error between the measurements of $\Delta\varepsilon^{II}_{re1}(t)$ and Eq. 17. By applying the similar procedure to subsequent

loading cycles the associated nonlinear VE parameters were evaluated in all loading cycles. Once all the nonlinear viscoelastic parameters were obtained, the irrecoverable strain response during the loading phase was obtained from Eq. 11 for Nth cycle as

$$\varepsilon_{irrec}^{N}(t) = \varepsilon_{cr}^{N}(t) - \varepsilon_{nve}^{N}(t) \tag{18}$$

where $N = I, II, III, \ldots$ = loading cycle number. This procedure leads to nonlinear VE parameters that are known at discrete stress levels (σ^N), and these parameters can be expressed as functions of stress through interpolation or regression.

2.5 Curve fitting-nonlinear VE parameters

Once all the nonlinear VE parameters were obtained at multiple stress levels, they were fitted with appropriate functions of stress. In this study we expressed the nonlinear VE parameters as smooth second order polynomial functions of effective or von Mises stress (σ_{eff}).

$$g_0 = 1 + \sum_{i}^{2} \alpha_i \left\langle \frac{\sigma_{eff}}{\sigma_0} - 1 \right\rangle^i \tag{19}$$

$$g_1 = 1 + \sum_{i}^{2} \beta_i \left\langle \frac{\sigma_{eff}}{\sigma_0} - 1 \right\rangle^i \tag{20}$$

$$g_2 = 1 + \sum_{i}^{2} \gamma_i \left\langle \frac{\sigma_{eff}}{\sigma_0} - 1 \right\rangle^i \tag{21}$$

$$a_\sigma = 1 + \sum_{i}^{2} \delta_i \left\langle \frac{\sigma_{eff}}{\sigma_0} - 1 \right\rangle^i \tag{22}$$

where

$$\langle x \rangle = \begin{cases} x & x > 0 \\ 0 & x \leq 0 \end{cases}$$

In our uniaxial MLCR tests, σ_{eff} is equal to the applied uniaxial stress in each loading cycle. The coefficients α_i, β_i, γ_i and δ_i ($i = 1,2$) were evaluated by fitting the Eqs. 19 - 22 to the obtained values of the parameters g_0, g_1, g_2 and a_σ, respectively, in all loading cycles

of MLCR tests on each trabecular bone sample. σ_0 (or σ^I) is the stress in the first loading cycle where linear viscoelastic parameters were determined for each sample. The above methodology for identification of nonlinear viscoelastic parameters is shown concisely as a flowchart in Fig. 2.

3 Results

3.1 MLCR experimental data

A total of 19 samples were subjected to MLCR tests and the range of BV/TV of the bone samples was 0.15 to 0.54. As discussed earlier our methods involved application of stress corresponding to eight different strain levels. Out of the 19 samples tested 4 failed (started displaying tertiary creep) in loading cycle VI, 4 in loading cycle VII and 9 in loading cycle VIII. Only 2 samples survived all eight stress levels. Typical creep-recovery responses along with the applied load cycles for two samples are shown in Fig. 3. These samples had a BV/TV of 0.25 and 0.46 and were consequently named as S25 and S46. Five cycles of loading (each followed by unloading) with the stress magnitudes of 0.64, 1.19, 1.77, 2.23, 2.43 MPa were applied to S25 and, similarly, six cycles with stress magnitudes of 1.75, 4.38, 7.45, 10.76, 14.06, 22.92 MPa were applied to S46 as shown in Figs. 3(a) and 3(b) respectively. The last cycle in each sample where tertiary creep or failure was observed was omitted in the analysis and also not shown in the figures. Results for all samples are provided in Table 1.

3.2 Viscoelastic recovery compliance

The viscoelastic recovery compliance was evaluated in all cycles using $\Delta\varepsilon^N_{re1}/\sigma^N$ (note that the numerator does not include irrecoverable strains) for all samples. Typical variation of compliance with time as well as with varying applied stress is shown in Figs. 4(a)-4(d) for samples S25, S33 and S46. The units for compliance are 1/MPa. In the first loading cycle, for the three typical samples, the viscoelastic recovery compliance increased by 11% (from 3.17×10^{-3} to 3.51×10^{-3}), 6% (from 1.40×10^{-3} to 1.48×10^{-3}) and 12% (from 1.00×10^{-3} to 1.12×10^{-3}) at 600 s (end of unloading phase) for samples S25, S33 and S46 respectively (Fig. 4). Compliance was found to increase with time in all loading cycles as expected in viscoelastic material. However, the compliance for trabecular bone also found to vary with stress indicating a nonlinear viscoelastic response. For sample S25, the compliance increased from 3.51×10^{-3} at the end of cycle I to 4.40×10^{-3} at the end of cycle V. For high density sample S46 the compliance decreased from 1.12×10^{-3} at the end of cycle I to 0.71×10^{-3} at the end of cycle VI. But in the sample S33, the compliance was found to first decrease from 1.48×10^{-3} at the end of cycle I to 1.25×10^{-3} at the end of loading cycle IV and then increase to 1.70×10^{-3} at the end of cycle VII. This stress dependent compliance behaviour is shown in Fig. 4(d) for the three samples. Figure 4(e) shows that compliance increases with stress for low BV/TV samples, decreases with stress for high BV/TV samples and first decreases with stress and then increases with stress for mid-BV/TV samples.

3.3 Nonlinear viscoelastic parameters

The stress-dependent nonlinear viscoelastic parameters, g_0, g_1, g_2 and a_σ, were evaluated for all 19 samples. Fig. 5(a) and 5(b) show the variation of these parameters for samples S25 and S46, respectively. The procedure assumes linear viscoelasticity in the first cycle

(initial apparent strain of 0.2%). Numerical values of stress-dependent nonlinear viscoelastic parameters along with other evaluated values are presented in Table 1 for all 19 samples. The results show that for sample S25 the values of g_0, g_2 and a_σ first decrease and then increase with the stress level, whereas the value of g_1 first increases slightly and then decreases slightly with the stress level (Fig. 5(a)). The product of $g_1 g_2$ which affects the transient response was also found to first decrease and then increase. These observations led us to the choice of a second order polynomial function to represent the nonlinear VE parameters as functions of effective stress. These second order functions produced coefficients of determination of r^2 = 0.97, 0.72, 0.98 and 0.69 for parameters g_0, g_1, g_2 and a_σ, respectively, as shown in Fig. 5(a).

For sample S46, Fig. 5(b), the parameters g_0, g_1, g_2 were found to decrease and then increase with the stress level, and a_σ was almost constant (≈ 1) and then decreased in the last stress cycle. The second order polynomial functions of effective stress produced r^2 values of 0.83, 0.90, 0.92, and 0.93 for g_0, g_1, g_2 and a_σ , respectively for sample S46. The increase in the values of g_0, g_1, g_2 or the product of $g_1 g_2$ essentially means that the trabecular bone material experiences viscoelastic softening (reduction of stiffness) and decrease of these parameters imply that the material experiences stiffening.

Figures. 6(a), 6(b), 6(c) and 6(d) show the variation of nonlinear VE parameters, g_0, g_1, g_2 and a_σ,respectively, which were expressed as polynomial functions of effective stress, for all samples. It can be seen that the variation described for two typical samples is largely followed by all.

3.4 Irrecoverable strains

The irrecoverable strain along with nonlinear viscoelastic (recoverable) strain response for samples S25 and S46 are shown in Figs. 7(a) and 7(b). The figures also show the measured experimental strain response which comprises of the recoverable and irrecoverable strain components (Eq. 1). The viscoelastic strain was found to recover fully (below 7 $\mu\varepsilon$) in under 10 minutes during the recovery phase of each loading cycle. Irrecoverable strains exist even at the end of the first loading cycle (stress level corresponding to strain of 0.2%) and were found to increase with stress. For sample S25, the irrecoverable strain increased to 0.20% by the end of cycle V from 0.03% in cycle I, Fig. 7(a), whereas for sample S46, it increased to 0.12% by the end of loading cycle VI from 0.03% in cycle I, Fig. 7(b). The irrecoverable strains in each loading cycle for all 19 samples are shown in Fig. 8(a).

There were no significant correlations found between the irrecoverable strains and BV/TV in the loading cycles I-IV. However, a weak but significant power law correlation ($y = 0.0757x^{-0.61}$, $r^2 = 0.34$, $p < 0.001$) in the cycle V with BV/TV was found. At loading cycles at higher stress, strong and significant power law relationships $y = 0.0177x^{-2.93}$ ($r^2 = 0.78$, $p < 0.001$) and $y = 0.0862x^{-1.78}$ ($r^2 = 0.73$, $p < 0.001$) were found between the irrecoverable strains and BV/TV in the cycles VI and VII, respectively.

4 Discussion

This study developed a novel methodology to evaluate time-dependent properties of trabecular bone. Our creep-recovery experiments at multiple stress levels demonstrate that the response of trabecular bone to mechanical forces is time-dependent and the strain always comprises of recoverable and irrecoverable components even at low stress levels. Our re-

sults show that the viscoelastic behaviour of trabecular bone varies nonlinearly with the applied stress.

Stress-dependence of creep response has been previously examined in studies on polymers and concretes (Lai and Bakker, 1995; Huang et al, 2011). In these studies the creep-recovery tests were conducted independently and involved long relaxation periods between stress cycles. We performed creep and recovery tests at varying load levels continuously without resting the sample in between the tests. We chose this protocol, as it was not apparent how long different trabecular bone samples would take to to fully recover from any loading cycle. The adopted methodology required the residual strains from the previous cycle to be taken into account when evaluating the response of the following loading cycle.

The identification of viscoelastic parameters constitutes a two-step process. In the first step, the Prony coefficients associated with linear viscoelastic response are determined for the loading cycle at the lowest stress level, and in second step the linear viscoelastic response with additional appropriate constitutive parameters is manipulated to match-up with the experimental response at multiple stress levels using nonlinear least square minimisation technique; thereby the corresponding constitutive parameters are evaluated at multiple load levels. A major strength of our methodology is that it permits separation of the recoverable response from the total strain response through the use of creep and recovery parts of the curves in each loading cycle. Thus, it is possible to assess accurately the viscoelastic response of trabecular bone. Linear viscoelastic properties were characterized by the Prony series based on the generalized 3-term Kelvin model at the lowest stress cycle (corresponding to 0.2% of applied static strain), assuming bone behaves linearly at this small strain. The nonlinear viscoelastic parameters were successfully fitted to polynomial functions which represent the parameters as continuous functions of stress levels. Previous studies have also

reported that the time-dependent behaviour of the trabecular bone is nonlinear (Deligianni et al, 1994; Bowman et al, 1994; Yamamoto et al, 2006; Quaglini et al, 2009).

The viscoelastic recovery compliance was found to vary with time as well as with the applied stress demonstrating the nonlinear stress-dependent viscoelastic response of trabecular bone (Fig. 4). The samples with medium BV/TV (e.g S33, Fig. 4(b)) show an initially decreasing and then increasing viscoelastic recovery compliance with increasing stress. This indicates that the sample first becomes stiffer and then experiences softening (stiffness degradation). This could be due to the reorganisation of the micro or ultrastructural components in the bone matrix to make it stiffer initially followed by localised buckling and/or damage of trabeculae causing softening. Nair et al (2014) conducted compressive tests on mineralized and non-mineralized collagen microfibrils at molecular level at different compressive stress levels and found that the elastic modulus of mineralized collagen fibril increases significantly (stiffening) as the applied compressive load increases whereas the nonmineralized samples showed reduced elastic modulus (higher deformability) with increase in load. Our study demonstrates that this stiffening at ultrastructural level translates to macro-level stiffening behaviour. Similarly, excessive deformation at molecular level may break the bonds between organic and inorganic phases which can result in micro-damage which manifests itself as softening at the apparent level. In general, for low BV/TV samples softening initiates at low stress levels (e.g. S25, Fig. 4(a)), whereas the high BV/TV samples indicate stiffening with little or no degradation even at the higher stress levels at which they were tested (Fig. 4(c)). Thus, micro/ultrastructural reorganisation and localised buckling and/or damage may make a varying contribution (with BV/TV playing an important role) to the apparent stiffening-softening behaviour with increasing stress. At higher strain levels, the collective effect of buckling and damage in the individual trabeculae will become dominant resulting in failure or tertiary creep. Previous studies have reported that

the presence of marrow may also result in hydraulic stiffening (Cowin, 1999) at higher strain-rates. However, the unconfined MLCR experiments in our study were conducted at relatively low strain rates (0.01 s^{-1}), and it is unlikely that marrow would have played a role in the observed stiffening phenomena. Kim et al (2012) reported that the post-creep unloading modulus is significantly higher than pre-creep loading modulus indicating that the stiffening of trabecular bone occurs under compressive creep, and authors attributed this behaviour to the possible reorganization of micro or ultrastructural components in the bone. Our study also found similar stiffening at first and then softening under compressive creep.

All samples showed similar convex shape (Fig. 6(a)) for parameter g_0, which affects the instantaneous response, depending on their BV/TV with the coefficients of determination (r^2) of the polynomial functions were in the range of 0.18 to 0.99. The product of the parameters g_1 and g_2 which affects the transient response, Fig. 6(e), produced the r^2 value in the range of 0.37-0.99. Some of the second order polynomial functions of g_0 and g_1g_2 for some samples were weakly correlated, however, all of the correlations were positive and showed an initially decreasing and then increasing trend, which implies decreasing and increasing trend in the instantaneous and transient responses (recoverable compliance), respectively, with increasing stress. These functions of stress-dependent parameters explain the stiffening-softening behaviour of trabecular bone well under compressive creep loading. The change in parameter a_σ shows the nonlinearity in the time-shift factor as a function of stress. The approximations using second order polynomial functions of stress were considered appropriate as we had only data points corresponding to 5 to 8 stress levels.

The outstanding fact about these approximations is that all the functions revealed a stiffening-softening behaviour for all trabecular bone samples with varying degrees of success. With increasing stress the parameter g_0 and the product g_1g_2 reduce to less than 1 indicating stiffening (or reduced compliance) followed by an increase beyond 1 indicat-

ing softening (or increased compliance) with the further increase in stress . This can be clearly seen Fig. 6 and it can be observed that the viscoelastic response of samples with lower BV/TV was significantly different from samples with higher BV/TV. In general for lower the BV/TV samples the parameters reach their minima and increase to greater than 1 rapidly, indicating quicker stiffening-softening behaviour with stress. For samples with higher BV/TV the same behaviour was observed to vary more slowly with stress. From our results, it appears BV/TV is a good predictor of nonlinear stress-dependent viscoelastic response of the trabecular bone.

Irrecoverable strains (Fig. 8(a)) were found to exist even at smaller load levels. These strains existed consistently in all the samples and were of similar magnitudes in their first loading cycles. We believe these strains occur due to the material being loaded to strains beyond its yield point in some localised regions and entering the realm of irreversible deformation. Kim et al (2012) reported that the residual strain, which they defined as strain that remain at the end of the unloading phase, of 1797 $\pm$ 1391 $\mu\varepsilon$ remained after 2 hours of strain recovery in the unloading phase when the plateau force corresponding to static strain of 2000 $\mu\varepsilon$ was applied in a creep test. Yamamoto et al (2006) also reported residual strains and found that their magnitude was of a similar magnitude to the applied static strain (515 $\pm$ 255 $\mu\varepsilon$ and 1565 $\pm$ 590 for applied static strains of 750 and 1500 $\mu\varepsilon$, respectively) at the end 35 hours of recovery period. From this they estimated that these residual strains will fully recover in 26 to 63 days. Our study concludes that these residual strains are, in fact, irrecoverable (permanent) strains and never recover *in vitro*. We applied plateau load only for 200 s, the resulting irrecoverable strain magnitudes at the end of unloading phase (600 s of strain recovery) were of the order of 242 $\mu\varepsilon$ to 1267 $\mu\varepsilon$ in the first loading cycle where applied plateau load corresponds to static strain of 2000 $\mu\varepsilon$, consistent with those observed in the previous studies (Yamamoto et al, 2006; Kim et al, 2012). However, *in vivo*, since

bone is a living tissue, microdamage (which is the cause of these permanent strains) is likely to be repaired and replaced by a newer bone material via remodelling. In fact, microdamage in bone acts as a stimulus for directing biological activity (Burr et al, 1985; Lee et al, 2002). The microdamage initiates at scales below the macroscopic porosity of the bone, and may be affected by intrinsic viscoelasticity of the tissue phase. The newly formed material due to bone remodelling may have less mineral which may increase compliance locally. The overall viscoelastic response at apparent level represents an average of old and new bone.

Kim et al (2012) also reported from their experimental creep tests that the loading creep rate (during plateau load) is significantly higher than the unloading creep rate (during strain recovery in unloading phase) in trabecular bone. This possibly indicates that the creep response during plateau loading contains evolution of not only recoverable strain but also some irreversible strain response. Our study validates this phenomenon and concludes that the creep response of the trabecular bone always contains both recoverable and irrecoverable responses even at smaller strains/stresses.

These irrecoverable strains at lower loading cycles (I-IV) were found to have no correlation with BV/TV. However, as the applied plateau loads increase in the higher loading cycles (V-VII) these strains strongly depend on BV/TV, Fig. 8(b). Samples with lower BV/TV experienced higher irreversible strains with power law relationships, and irreversible strains decreased with the increasing BV/TV at the same applied strain level, Fig. 8(b).

The mechanisms driving the viscoelastic behaviour in trabecular bone are not yet completely understood. It has been speculated that the individual constituents at different hierarchical levels in the trabecular bone and its microstructure contribute to the viscoelastic behaviour at the specimen level. Linde (1994) pointed out that the viscoelastic response of trabecular bone may depend on both the presence of marrow within the tissue and properties of the tissue itself, and Bowman et al (1999) suggested that the collagen phase is responsible

for the creep behaviour of the trabecular bone. Nair et al (2014) suggested that extrafibrillar mineralization is mandatory along with intrafibrillar mineralization to provide the required bone mechanical properties. Further investigations are required to explicitly quantify the contributions of individual constituents to the apparent level viscoelastic behaviour of bone. However, from our results, it is evident that the BV/TV plays a major role in predicting the apparent level viscoelastic behaviour (Manda et al, 2016).

This work can be incorporated in finite element (FE) programs by coding a user defined material (UMAT) subroutine based on Schapery's single integral model (Schapery, 1969), which is not generally available in commercial FE packages. The linear Prony coefficients and the stress dependent nonlinear VE parameters reported in Table 1 will act as input to the UMAT. The nonlinear VE parameters need to be supplied as smooth functions of stress (Eqs. 19 - 22).

Our study also has a few limitations. Firstly, it is not possible in practice to perform ideal creep-recovery experiments, and in our tests the time intervals during the ramp loading and unloading are finite (1 s to reach 1.0% strain with the strain rate of 0.01 s^{-1}). Small viscoelastic deformations are likely to occur during the ramp loading phase; it may be possible to include these in a more elaborate model. In this study finite ramp loading/unloading was treated as instantaneous in our material model; we believe this assumption has negligible effect on the evaluated material parameters. Our creep tests were performed with the plateau load holding time of 200 s which we believe is sufficiently long in comparison to the ramp loading/unloading time it will have a negligible effect on the measured creep response. As in many previous studies our experiments were performed at room temperature. It is possible that increase in temperature to 37 °C may have a small effect on the creep behaviour; currently the published data to confirm or invalidate this is limited.

5 Compliance with Ethical Standards

The proximal bovine femora used in this study were obtained from a local abattoir.

6 Funding

This study was funded by the Engineering and Physical Sciences Research Council (grant number EP/K036939/1).

7 Conflict of Interest

None of the authors have any conflicts of interest to report with respect to the material contained in this manuscript.

Acknowledgements The authors are grateful to the Engineering and Physical Sciences Research Council (EPSRC) grant EP/K036939/1.

References

Bowman SM, Keaveny TM, Gibson LJ, Hayes WC, McMahon TA (1994) Compressive creep behavior of bovine trabecular bone. Journal of Biomechanics 27(3):301–305, 307–310

Bowman SM, Guo XE, Cheng DW, Keaveny TM, Gibson LJ, Hayes WC, McMahon TA (1998) Creep contributes to the fatigue behavior of bovine trabecular bone. Journal of Biomechanical Engineering 120(5):647–654

Bowman SM, Gibson LJ, Hayes WC, McMahon TA (1999) Results from demineralized bone creep tests suggest that collagen is responsible for the creep behavior of bone. Journal of Biomechanical Engineering 121(2):253–258

544 Bredbenner TL, Davy DT (2006) The effect of damage on the viscoelastic behavior of hu-
545 man vertebral trabecular bone. Journal of Biomechanical Engineering 128(4):473–480
546 Burr DB, Martin RB, Schaffler MB, Radin EL (1985) Bone remodeling in response to in
547 vivo fatigue microdamage. Journal of Biomechanics 18(3):189–200
548 Christensen RM (1980) Nonlinear theory of viscoelasticity for application to elastomers.
549 Journal of Applied Mechanics, Transactions ASME 47(4):762–768
550 Cowin SC (1999) Bone poroelasticity. Journal of Biomechanics 32(3):217–238
551 Currey JD (1986) Power law models for the mechanical properties of cancellous bone. En-
552 gineering in medicine 15(3):153–154
553 Deligianni DD, Maris A, Missirlis YF (1994) Stress relaxation behaviour of trabecular bone
554 specimens. Journal of Biomechanics 27(12):1469–1476
555 Dillard DA, Straight MR, Brinson HF (1987) The nonlinear viscoelastic characterization of
556 graphite/epoxy composites. Polymer Engineering & Science 27(2):116–123
557 Findley W, Lai J, Onaran K (1976) Creep and relaxation of nonlinear viscoelastic materials,
558 with an introduction to linear viscoelasticity. North-Holland series in applied mathematics
559 and mechanics, North-Holland Pub. Co.
560 Goffin JM, Pankaj P, Simpson AH (2013) The importance of lag screw position for the
561 stabilization of trochanteric fractures with a sliding hip screw: A subject-specific finite
562 element study. Journal of Orthopaedic Research 31(4):596–600
563 Guedes RM, Simes JA, Morais JL (2006) Viscoelastic behaviour and failure of bovine can-
564 cellous bone under constant strain rate. Journal of Biomechanics 39(1):49–60
565 Huang C, Abu Al-Rub RK, Masad EA, Little DN, Airey GD (2011) Numerical implemen-
566 tation and validation of a nonlinear viscoelastic and viscoplastic model for asphalt mixes.
567 International Journal of Pavement Engineering 12(4):433–447

568 Keaveny TM, Pinilla TP, Crawford RP, Kopperdahl DL, Lou A (1997) Systematic and ran-
569 dom errors in compression testing of trabecular bone. Journal of Orthopaedic Research
570 15(1):101–110
571 Keaveny TM, Morgan EF, Niebur GL, Yeh OC (2001) Biomechanics of trabecular bone.
572 Annual Review of Biomedical Engineering 3:307–333
573 Kim DG, Navalgund AR, Tee BC, Noble GJ, Hart RT, Lee HR (2012) Increased variability
574 of bone tissue mineral density resulting from estrogen deficiency influences creep behav-
575 ior in a rat vertebral body. Bone 51(5):868 – 875
576 Kim DG, Huja SS, Navalgund A, DAtri A, Tee B, Reeder S, Lee HR (2013) Effect of
577 estrogen deficiency on regional variation of a viscoelastic tissue property of bone. Journal
578 of Biomechanics 46(1):110 – 115
579 Knauss WG, Emri IJ (1981) Non-linear viscoelasticity based on free volume consideration.
580 Computers and Structures 13(1-3):123–128
581 Kopperdahl DL, Keaveny TM (1998) Yield strain behavior of trabecular bone. Journal of
582 Biomechanics 31(7):601–608
583 Lai J, Bakker A (1995) An integral constitutive equation for nonlinear plasto-viscoelastic
584 behavior of high-density polyethylene. Polymer Engineering & Science 35(17):1339–
585 1347
586 Lee TC, Staines A, Taylor D (2002) Bone adaptation to load: Microdamage as a stimulus
587 for bone remodelling. Journal of anatomy 201(6):437–446
588 Levrero-Florencio F, Margetts L, Sales E, Xie S, Manda K, Pankaj P (2016) Evaluating
589 the macroscopic yield behaviour of trabecular bone using a nonlinear homogenisation
590 approach. Journal of the Mechanical Behavior of Biomedical Materials 61:384–396
591 Linde F (1994) Elastic and viscoelastic properties of trabecular bone by a compression test-
592 ing approach. Danish medical bulletin 41(2):119–138

593 Linde F, Hvid I, Pongsoipetch B (1989) Energy absorptive properties of human trabecular
594 bone specimens during axial compression. Journal of Orthopaedic Research 7(3):432–
595 439
596 Lou YC, Schapery RA (1971) Viscoelastic characterization of a nonlinear fiber- reinforced
597 plastic. Journal of Composite Materials 5:208–234
598 Manda K, Xie S, Wallace RJ, Levrero-Florencio F, Pankaj P (2016) Linear viscoelasticity -
599 bone volume fraction relationships of bovine trabecular bone. Biomechanics and Model-
600 ing in Mechanobiology pp 1–10, article in Press, DOI:10.1007/s10237-016-0787-0
601 Morgan EF, Yeh OC, Chang WC, Keaveny TM (2001) Nonlinear behavior of trabecular
602 bone at small strains. Journal of Biomechanical Engineering 123(1):1–9
603 Morgan EF, Bayraktar HH, Keaveny TM (2003) Trabecular bone modulus density relation-
604 ships depend on anatomic site. Journal of Biomechanics 36(7):897 – 904
605 Nair AK, Gautieri A, Buehler MJ (2014) Role of intrafibrillar collagen mineralization in
606 defining the compressive properties of nascent bone. Biomacromolecules 15(7):2494–
607 2500
608 Nordin L, Varna J (2005) Methodology for parameter identification in nonlinear viscoelastic
609 material model. Mechanics of Time-Dependent Materials 9(4):259–280
610 Norman TL, Ackerman ES, Smith TS, Gruen TA, Yates AJ, Blaha JD, Kish VL (2006)
611 Cortical bone viscoelasticity and fixation strength of press-fit femoral stems: An in-vitro
612 model. Journal of Biomechanical Engineering 128(1):13–17
613 Phillips A, Pankaj P, May F, Taylor K, Howie C, Usmani A (2006) Constitutive models for
614 impacted morsellised cortico-cancellous bone. Biomaterials 27(9):2162–2170
615 Pollintine P, Luo J, Offa-Jones B, Dolan P, Adams MA (2009) Bone creep can cause pro-
616 gressive vertebral deformity. Bone 45(3):466–472

617 Provenzano PP, Lakes RS, Corr DT, Vanderby Jr R (2002) Application of nonlinear
618 viscoelastic models to describe ligament behavior. Biomechanics and Modeling in
619 Mechanobiology 1(1):45–57
620 Quaglini V, Russa VL, Corneo S (2009) Nonlinear stress relaxation of trabecular bone.
621 Mechanics Research Communications 36(3):275–283
622 Rachner TD, Khosla S, Hofbauer LC (2011) Osteoporosis: Now and the future. The Lancet
623 377(9773):1276–1287
624 Schapery RA (1969) On characterization of nonlinear viscoelastic materials. Polymer Eng
625 & Science 9(4):295–310
626 Schapery RA (1997) Nonlinear viscoelastic and viscoplastic constitutive equations based on
627 thermodynamics. Mechanics Time-Dependent Materials 1(2):209–240
628 Schoenfeld CM, Lautenschlager EP, Meyer PR (1974) Mechanical properties of human can-
629 cellous bone in the femoral head. Medical and Biological Engineering 12(3):313–317
630 Singh M, Nagrath AR, Maini PS (1970) Changes in trabecular pattern of the upper end
631 of the femur as an index of osteoporosis. Journal of Bone and Joint Surgery - Series A
632 52(3):457–467
633 Smart J, Williams J (1972) A comparison of single-integral non-linear viscoelasticity theo-
634 ries. Journal of the Mechanics and Physics of Solids 20(5):313 – 324
635 Yamamoto E, Paul Crawford R, Chan DD, Keaveny TM (2006) Development of residual
636 strains in human vertebral trabecular bone after prolonged static and cyclic loading at low
637 load levels. Journal of Biomechanics 39(10):1812–1818
638 Zilch H, Rohlmann A, Bergmann G, Koelbel R (1980) Material properties of femoral can-
639 cellous bone in axial loading. part ii: Time-dependent properties. Archives of Orthopaedic
640 and Traumatic Surgery 97(4):257–262

Table 1: The nonlinear VE parameters along with linear Prony coefficients and irrecoverable strains at multiple stress levels for all 19 samples. BV/TV is the bone volume fraction, D_0 is the instantaneous compliance in 1/MPa, D_n (n = 1, 2, 3) are transient compliance coefficients in 1/MPa, and λ_n (n = 1, 2, 3) are reciprocal of nth retardation time in Prony series in s^{-1}, ε_{static} is the applied static strain in each loading cycle, σ^N is the stress corresponding to plateau stress in the Nth loading cycle in MPa. Parameters g_0, g_1, g_2, a_σ are stress-dependent nonlinear VE parameters and ε_{irrec} is the irrecoverable strain exist at the end of each loading cycle.

BV/TV	Linear Prony coefficients at σ^I	Cycle No.	ε_{static}[%]	σ^N[MPa]	Nonlinear VE parameters				ε_{irrec}[%]
					g_0	g_1	g_2	a_σ	
0.15	$\begin{bmatrix} D_0 \\ D_1 \\ D_2 \\ D_3 \\ \lambda_1 \\ \lambda_2 \\ \lambda_3 \end{bmatrix} = \begin{bmatrix} 6.40e-03 \\ 5.48e-04 \\ 3.24e-04 \\ 2.97e-04 \\ 8.64e-03 \\ 8.64e-01 \\ 9.31e-02 \end{bmatrix}$	*I*	0.20	0.36	1.00	1.00	1.00	1.00	0.041
		II	0.40	0.66	0.91	1.06	0.59	0.78	0.067
		III	0.60	0.94	0.94	1.03	0.67	0.82	0.104
		IV	0.80	1.17	0.99	1.01	0.82	0.85	0.158
		V	1.00	1.35	1.10	0.96	0.84	0.91	0.237
0.19	$\begin{bmatrix} D_0 \\ D_1 \\ D_2 \\ D_3 \\ \lambda_1 \\ \lambda_2 \\ \lambda_3 \end{bmatrix} = \begin{bmatrix} 3.44e-03 \\ 1.85e-04 \\ 1.25e-04 \\ 2.47e-04 \\ 6.51e-01 \\ 4.12e-02 \\ 3.57e-03 \end{bmatrix}$	*I*	0.20	0.64	1.00	1.00	1.00	1.00	0.024
		II	0.40	1.24	0.89	0.85	0.94	0.88	0.045
		III	0.60	1.89	0.87	0.89	1.02	0.92	0.076
		IV	0.80	2.44	0.85	0.86	1.50	0.86	0.150

Continued on next page...

BV/TV	Linear Prony coefficients at σ^I	Cycle No.	$\varepsilon_{static}[\%]$	σ^N[MPa]	Nonlinear VE parameters				$\varepsilon_{irrec}[\%]$
					g_0	g_1	g_2	a_σ	
		V	1.00	2.74	0.90	0.85	1.51	0.90	0.230
0.21	$\begin{bmatrix} D_0 \\ D_1 \\ D_2 \\ D_3 \\ \lambda_1 \\ \lambda_2 \\ \lambda_3 \end{bmatrix} = \begin{bmatrix} 3.42e-03 \\ 3.39e-04 \\ 3.29e-04 \\ 1.64e-04 \\ 6.20e-03 \\ 2.42e+00 \\ 1.12e-01 \end{bmatrix}$	I	0.20	0.60	1.00	1.00	1.00	1.00	0.026
		II	0.40	1.16	0.90	1.05	0.84	0.69	0.041
		III	0.60	1.73	0.87	1.06	0.82	0.69	0.062
		IV	0.80	2.38	0.85	1.05	0.91	0.73	0.099
		V	1.00	2.82	0.88	1.04	1.11	0.73	0.161
0.25	$\begin{bmatrix} D_0 \\ D_1 \\ D_2 \\ D_3 \\ \lambda_1 \\ \lambda_2 \\ \lambda_3 \end{bmatrix} = \begin{bmatrix} 3.52e-03 \\ 1.31e-04 \\ 2.63e-04 \\ 1.30e-04 \\ 7.57e-02 \\ 6.44e-03 \\ 5.68e-01 \end{bmatrix}$	I	0.20	0.64	1.00	1.00	1.00	1.00	0.032
		II	0.40	1.20	0.90	1.02	0.82	0.79	0.049
		III	0.60	1.77	0.91	1.05	0.96	0.75	0.084
		IV	0.80	2.23	0.98	1.04	1.19	0.74	0.140
		V	1.00	2.43	1.06	1.01	1.44	0.81	0.209
0.26	$\begin{bmatrix} D_0 \\ D_1 \\ D_2 \\ D_3 \\ \lambda_1 \\ \lambda_2 \\ \lambda_3 \end{bmatrix} = \begin{bmatrix} 2.68e-03 \\ 1.75e-04 \\ 1.33e-04 \\ 1.66e-04 \\ 7.77e-03 \\ 1.15e-01 \\ 1.06e+00 \end{bmatrix}$	I	0.20	0.80	1.00	1.00	1.00	1.00	0.057
		II	0.40	1.65	0.78	0.94	0.64	0.91	0.089
		III	0.60	2.48	0.77	0.99	0.71	0.88	0.116
		IV	0.80	3.28	0.81	0.90	0.65	0.96	0.142

Continued on next page...

BV/TV	Linear Prony coefficients at σ^I	Cycle No.	ε_{static}[%]	σ^N[MPa]	Nonlinear VE parameters				ε_{irrec}[%]
					g_0	g_1	g_2	a_σ	
		V	1.00	4.01	0.83	0.89	0.79	0.97	0.186
		VI	1.50	6.50	0.82	1.01	1.86	0.86	0.960
		VII	2.00	3.62	1.02	0.94	2.14	0.96	1.041
0.33	$\begin{bmatrix} D_0 \\ D_1 \\ D_2 \\ D_3 \\ \lambda_1 \\ \lambda_2 \\ \lambda_3 \end{bmatrix} = \begin{bmatrix} 1.75e-03 \\ 7.46e-05 \\ 1.11e-04 \\ 6.68e-05 \\ 9.87e-03 \\ 1.02e+00 \\ 1.21e-01 \end{bmatrix}$	*I*	0.20	1.19	1.00	1.00	1.00	1.00	0.065
		II	0.40	2.76	0.66	0.93	0.84	0.98	0.076
		III	0.60	4.58	0.63	0.94	0.74	0.99	0.083
		IV	0.80	6.40	0.62	0.92	0.71	0.98	0.091
		V	1.00	8.18	0.62	0.95	0.67	0.99	0.100
		VI	1.50	13.37	0.75	0.92	1.32	0.95	0.442
		VII	2.00	11.13	0.78	0.92	1.53	0.96	0.526
0.35	$\begin{bmatrix} D_0 \\ D_1 \\ D_2 \\ D_3 \\ \lambda_1 \\ \lambda_2 \\ \lambda_3 \end{bmatrix} = \begin{bmatrix} 1.60e-03 \\ 1.14e-04 \\ 6.45e-05 \\ 8.35e-05 \\ 7.64e-03 \\ 9.41e-02 \\ 7.05e-01 \end{bmatrix}$	*I*	0.20	1.31	1.00	1.00	1.00	1.00	0.039
		II	0.40	2.69	0.84	1.14	0.71	0.67	0.057
		III	0.60	4.09	0.84	1.08	0.60	0.78	0.072
		IV	0.80	5.59	0.82	1.00	0.57	0.87	0.075
		V	1.00	7.50	0.78	1.00	0.37	0.93	0.109
		VI	1.50	13.01	0.70	1.02	0.66	0.80	0.214
0.35	$\begin{bmatrix} D_0 \\ D_1 \\ D_2 \\ D_3 \\ \lambda_1 \\ \lambda_2 \\ \lambda_3 \end{bmatrix} = \begin{bmatrix} 2.16e-03 \\ 1.41e-04 \\ 1.43e-04 \\ 1.11e-04 \\ 6.41e-03 \\ 1.41e+00 \\ 1.22e-01 \end{bmatrix}$	*I*	0.20	0.94	1.00	1.00	1.00	1.00	0.047
		II	0.40	2.16	0.70	1.02	0.84	0.84	0.077
		III	0.60	3.46	0.67	1.03	0.80	0.85	0.097
		IV	0.80	4.67	0.65	1.02	0.75	0.86	0.118

Continued on next page...

BV/TV	Linear Prony coefficients at σ^I	Cycle No.	ε_{static}[%]	σ^N[MPa]	Nonlinear VE parameters				ε_{irrec}[%]
					g_0	g_1	g_2	a_σ	
		V	1.00	6.04	0.63	1.02	0.72	0.87	0.135
		VI	1.50	10.67	0.62	1.04	0.82	0.80	0.406
		VII	2.00	11.83	0.62	1.03	0.94	0.79	0.522
0.36	$\begin{bmatrix} D_0 \\ D_1 \\ D_2 \\ D_3 \\ \lambda_1 \\ \lambda_2 \\ \lambda_3 \end{bmatrix} = \begin{bmatrix} 2.07e-03 \\ 1.48e-04 \\ 1.52e-04 \\ 1.55e-04 \\ 1.63e-01 \\ 1.07e-02 \\ 1.75e+00 \end{bmatrix}$	*I*	0.20	0.98	1.00	1.00	1.00	1.00	0.073
		II	0.40	2.12	0.71	1.20	0.45	0.70	0.087
		III	0.60	3.67	0.65	1.02	0.43	0.87	0.112
		IV	0.80	5.28	0.62	0.95	0.41	0.93	0.128
		V	1.00	7.02	0.59	0.89	0.40	0.97	0.144
		VI	1.50	12.73	0.54	1.00	0.42	0.89	0.244
		VII	2.00	16.68	0.45	1.01	0.75	0.79	0.377
0.39	$\begin{bmatrix} D_0 \\ D_1 \\ D_2 \\ D_3 \\ \lambda_1 \\ \lambda_2 \\ \lambda_3 \end{bmatrix} = \begin{bmatrix} 1.53e-03 \\ 1.07e-04 \\ 1.07e-04 \\ 8.45e-05 \\ 6.37e-03 \\ 1.27e+00 \\ 1.23e-01 \end{bmatrix}$	*I*	0.20	1.33	1.00	1.00	1.00	1.00	0.058
		II	0.40	2.92	0.76	0.83	0.76	0.97	0.066
		III	0.60	4.79	0.67	1.02	0.78	0.83	0.076
		IV	0.80	6.69	0.63	1.05	0.83	0.75	0.089
		V	1.00	8.53	0.65	1.07	0.64	0.79	0.111
		VI	1.50	14.81	0.66	1.02	0.56	0.86	0.288
		VII	2.00	17.19	0.60	1.04	1.01	0.77	0.458
0.40	$\begin{bmatrix} D_0 \\ D_1 \\ D_2 \\ D_3 \\ \lambda_1 \\ \lambda_2 \\ \lambda_3 \end{bmatrix} = \begin{bmatrix} 2.88e-03 \\ 2.36e-04 \\ 5.01e-04 \\ 2.56e-04 \\ 1.12e-02 \\ 2.57e+00 \\ 1.54e-01 \end{bmatrix}$	*I*	0.20	0.71	1.00	1.00	1.00	1.00	0.127
		II	0.40	1.65	0.46	0.89	0.51	0.97	0.170
		III	0.60	2.95	0.44	0.87	0.41	0.96	0.201
		IV	0.80	4.32	0.43	0.90	0.40	0.98	0.220

Continued on next page...

BV/TV	Linear Prony coefficients at σ^I	Cycle No.	ε_{static}[%]	σ^N[MPa]	Nonlinear VE parameters				ε_{irrec}[%]
					g_0	g_1	g_2	a_σ	
		V	1.00	5.74	0.43	0.91	0.34	0.99	0.227
		VI	1.50	11.56	0.39	0.92	0.36	0.94	0.346
		VII	2.00	14.98	0.39	0.90	0.33	0.97	0.491
0.40	$\begin{bmatrix} D_0 \\ D_1 \\ D_2 \\ D_3 \\ \lambda_1 \\ \lambda_2 \\ \lambda_3 \end{bmatrix} = \begin{bmatrix} 2.69e-03 \\ 9.10e-05 \\ 1.02e-04 \\ 1.26e-04 \\ 1.55e-01 \\ 9.68e-03 \\ 1.13e+00 \end{bmatrix}$	*I*	0.20	0.77	1.00	1.00	1.00	1.00	0.085
		II	0.40	2.13	0.52	0.85	0.73	0.96	0.109
		III	0.60	3.69	0.47	0.88	0.67	0.98	0.126
		IV	0.80	5.35	0.43	0.96	0.70	0.91	0.141
		V	1.00	7.11	0.43	0.88	0.60	0.98	0.160
		VI	1.50	13.69	0.37	0.99	0.69	0.89	0.295
		VII	2.00	17.41	0.38	1.01	0.95	0.87	0.550
0.42	$\begin{bmatrix} D_0 \\ D_1 \\ D_2 \\ D_3 \\ \lambda_1 \\ \lambda_2 \\ \lambda_3 \end{bmatrix} = \begin{bmatrix} 1.47e-03 \\ 1.09e-04 \\ 8.72e-05 \\ 7.91e-05 \\ 2.81e+00 \\ 8.63e-03 \\ 1.76e-01 \end{bmatrix}$	*I*	0.20	1.37	1.00	1.00	1.00	1.00	0.037
		II	0.40	2.97	0.73	1.03	0.98	0.83	0.054
		III	0.60	4.74	0.71	1.04	0.86	0.82	0.059
		IV	0.80	6.57	0.69	1.04	0.82	0.84	0.079
		V	1.00	8.44	0.66	1.03	0.85	0.85	0.091
		VI	1.50	14.45	0.67	0.91	0.68	0.96	0.158
		VII	2.00	19.20	0.63	1.01	0.88	0.86	0.301
0.43	$\begin{bmatrix} D_0 \\ D_1 \\ D_2 \\ D_3 \\ \lambda_1 \\ \lambda_2 \\ \lambda_3 \end{bmatrix} = \begin{bmatrix} 1.94e-03 \\ 1.19e-04 \\ 1.75e-04 \\ 9.27e-05 \\ 7.85e-01 \\ 7.38e-03 \\ 9.59e-02 \end{bmatrix}$	*I*	0.20	1.08	1.00	1.00	1.00	1.00	0.066
		II	0.40	2.39	0.67	1.09	0.60	0.74	0.096
		III	0.60	3.88	0.63	1.03	0.59	0.80	0.118
		IV	0.80	5.54	0.60	1.05	0.55	0.77	0.141

Continued on next page...

BV/TV	Linear Prony coefficients at σ^I	Cycle No.	ε_{static}[%]	σ^N[MPa]	Nonlinear VE parameters				ε_{irrec}[%]
					g_0	g_1	g_2	a_σ	
		V	1.00	7.22	0.61	0.89	0.52	0.96	0.146
		VI	1.50	13.04	0.57	1.01	0.42	0.84	0.268
		VII	2.00	16.91	0.55	1.00	0.51	0.85	0.406
		$VIII$	2.50	20.56	0.56	1.00	0.57	0.86	0.608
0.43	$\begin{bmatrix} D_0 \\ D_1 \\ D_2 \\ D_3 \\ \lambda_1 \\ \lambda_2 \\ \lambda_3 \end{bmatrix} = \begin{bmatrix} 9.40e-04 \\ 3.67e-05 \\ 6.46e-05 \\ 6.43e-05 \\ 1.06e-01 \\ 6.74e-03 \\ 9.59e-01 \end{bmatrix}$	I	0.20	2.13	1.00	1.00	1.00	1.00	0.042
		II	0.40	4.75	0.74	1.09	0.70	0.73	0.057
		III	0.60	7.96	0.67	1.08	0.64	0.70	0.074
		IV	0.80	11.29	0.64	1.07	0.62	0.75	0.088
		V	1.00	14.65	0.61	1.06	0.68	0.78	0.102
		VI	1.50	24.26	0.66	1.04	0.75	0.72	0.180
0.46	$\begin{bmatrix} D_0 \\ D_1 \\ D_2 \\ D_3 \\ \lambda_1 \\ \lambda_2 \\ \lambda_3 \end{bmatrix} = \begin{bmatrix} 1.16e-03 \\ 4.19e-05 \\ 5.82e-05 \\ 8.91e-05 \\ 6.99e-02 \\ 6.48e-03 \\ 6.75e-01 \end{bmatrix}$	I	0.20	1.75	1.00	1.00	1.00	1.00	0.037
		II	0.40	4.38	0.68	0.92	0.78	1.00	0.043
		III	0.60	7.45	0.61	0.89	0.69	0.97	0.049
		IV	0.80	10.77	0.57	0.88	0.62	0.97	0.056
		V	1.00	14.06	0.56	0.83	0.62	0.98	0.060
		VI	1.50	22.92	0.53	1.01	0.60	0.79	0.121
0.52	$\begin{bmatrix} D_0 \\ D_1 \\ D_2 \\ D_3 \\ \lambda_1 \\ \lambda_2 \\ \lambda_3 \end{bmatrix} = \begin{bmatrix} 2.29e-03 \\ 1.74e-04 \\ 2.03e-04 \\ 1.60e-04 \\ 1.50e+00 \\ 6.85e-03 \\ 1.29e-01 \end{bmatrix}$	I	0.20	0.89	1.00	1.00	1.00	1.00	0.095
		II	0.40	2.25	0.48	1.13	0.63	0.66	0.138
		III	0.60	3.87	0.43	1.09	0.60	0.69	0.175

Continued on next page...

BV/TV	Linear Prony coefficients at σ^I	Cycle No.	$\varepsilon_{static}[\%]$	σ^N[MPa]	Nonlinear VE parameters				$\varepsilon_{irrec}[\%]$
					g_0	g_1	g_2	a_σ	
		IV	0.80	5.62	0.42	1.08	0.49	0.74	0.210
		V	1.00	7.54	0.43	0.76	0.50	0.97	0.239
		VI	1.50	15.62	0.36	1.05	0.41	0.76	0.364
		VII	2.00	20.88	0.36	1.03	0.32	0.82	0.447
		VIII	2.50	26.56	0.33	1.03	0.53	0.73	0.656
0.53	$\begin{bmatrix} D_0 \\ D_1 \\ D_2 \\ D_3 \\ \lambda_1 \\ \lambda_2 \\ \lambda_3 \end{bmatrix} = \begin{bmatrix} 9.05e-04 \\ 4.26e-05 \\ 3.35e-05 \\ 4.21e-05 \\ 6.32e-01 \\ 6.40e-02 \\ 5.54e-03 \end{bmatrix}$	*I*	0.20	2.22	1.00	1.00	1.00	1.00	0.033
		II	0.40	5.03	0.79	0.81	0.95	0.92	0.048
		III	0.60	8.02	0.75	0.84	0.88	0.92	0.059
		IV	0.80	11.05	0.73	0.83	0.90	0.94	0.073
		V	1.00	14.10	0.71	0.87	0.91	0.96	0.085
		VI	1.50	23.66	0.67	1.00	1.07	0.78	0.174
		VII	2.00	30.13	0.75	1.01	0.90	0.86	0.310
0.54	$\begin{bmatrix} D_0 \\ D_1 \\ D_2 \\ D_3 \\ \lambda_1 \\ \lambda_2 \\ \lambda_3 \end{bmatrix} = \begin{bmatrix} 1.36e-03 \\ 8.02e-05 \\ 6.44e-05 \\ 6.17e-05 \\ 8.56e-01 \\ 8.64e-03 \\ 9.62e-02 \end{bmatrix}$	*I*	0.20	1.49	1.00	1.00	1.00	1.00	0.050
		II	0.40	4.00	0.58	1.06	0.71	1.00	0.058
		III	0.60	7.38	0.50	1.11	0.48	1.00	0.061
		IV	0.80	11.01	0.45	0.90	0.60	0.98	0.065
		V	1.00	14.66	0.45	0.87	0.47	1.00	0.074
		VI	1.50	24.90	0.42	0.96	0.49	0.88	0.129

641

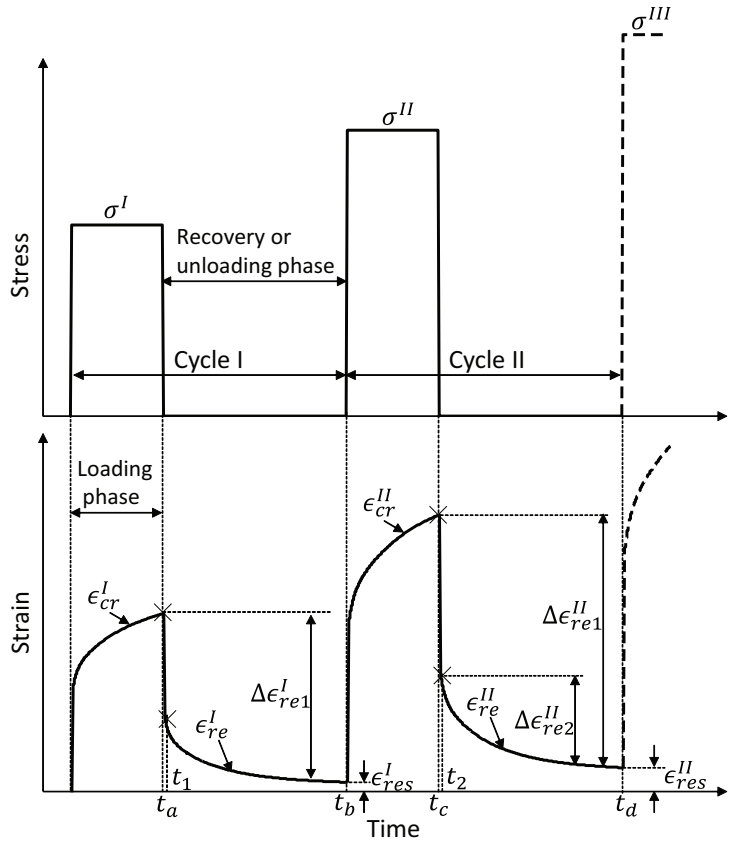

Fig. 1 A schematic representation of experimental creep and recovery tests at multiple load levels

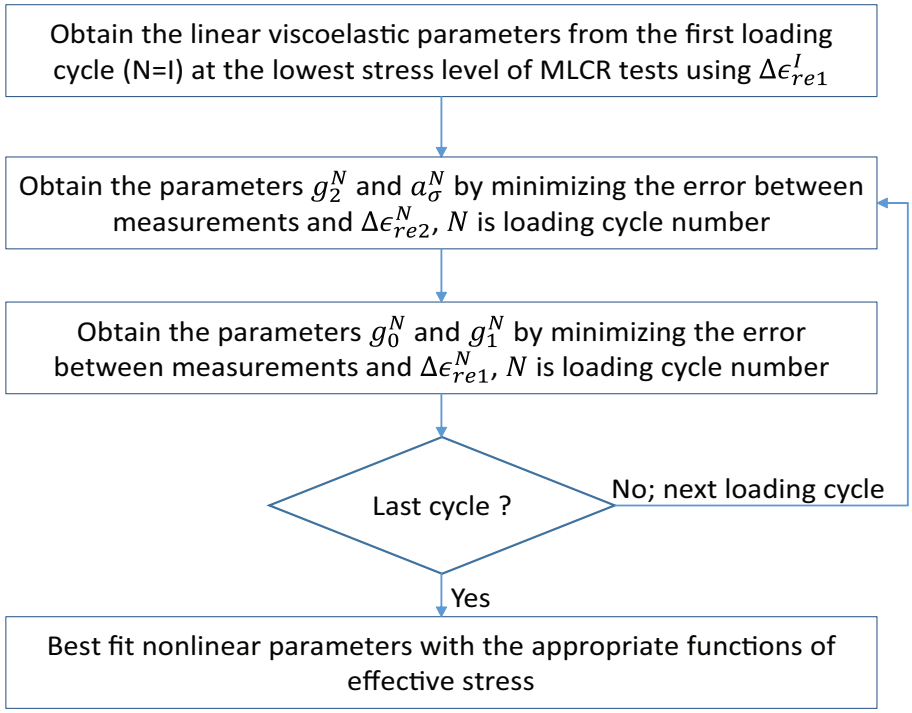

Fig. 2 Methodology for estimation of nonlinear viscoelastic parameters of trabecular bone

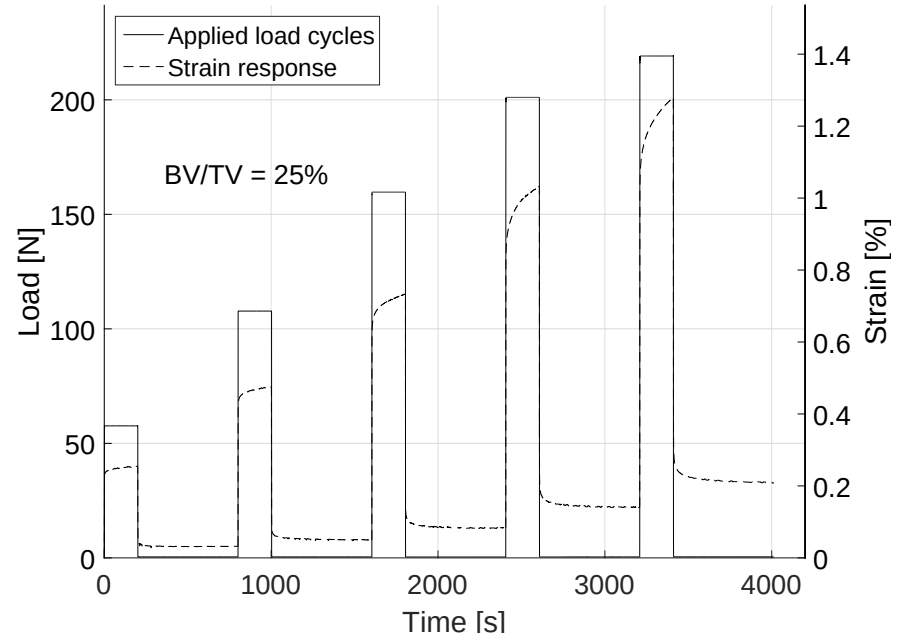

(a)

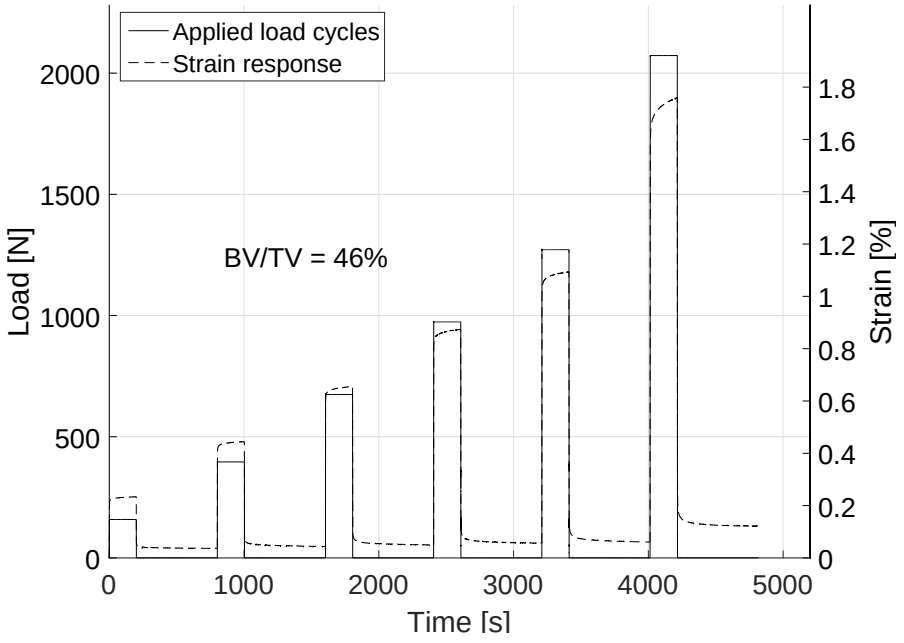

(b)

Fig. 3 Experimental creep-recovery responses from MLCR tests along with the applied load levels on two typical samples of (a) BV/TV = 0.25 and (b) BV/TV = 0.46. In each cycle plateau load was held constant for 200 s and strain recovery was measured for another 600 s. The load or stress levels in each of the loading cycle I, II, III, IV, V, and VI correspond to the static strains of 0.2%, 0.4%, 0.6%, 0.8%, 1.0%, and 1.5%, respectively.

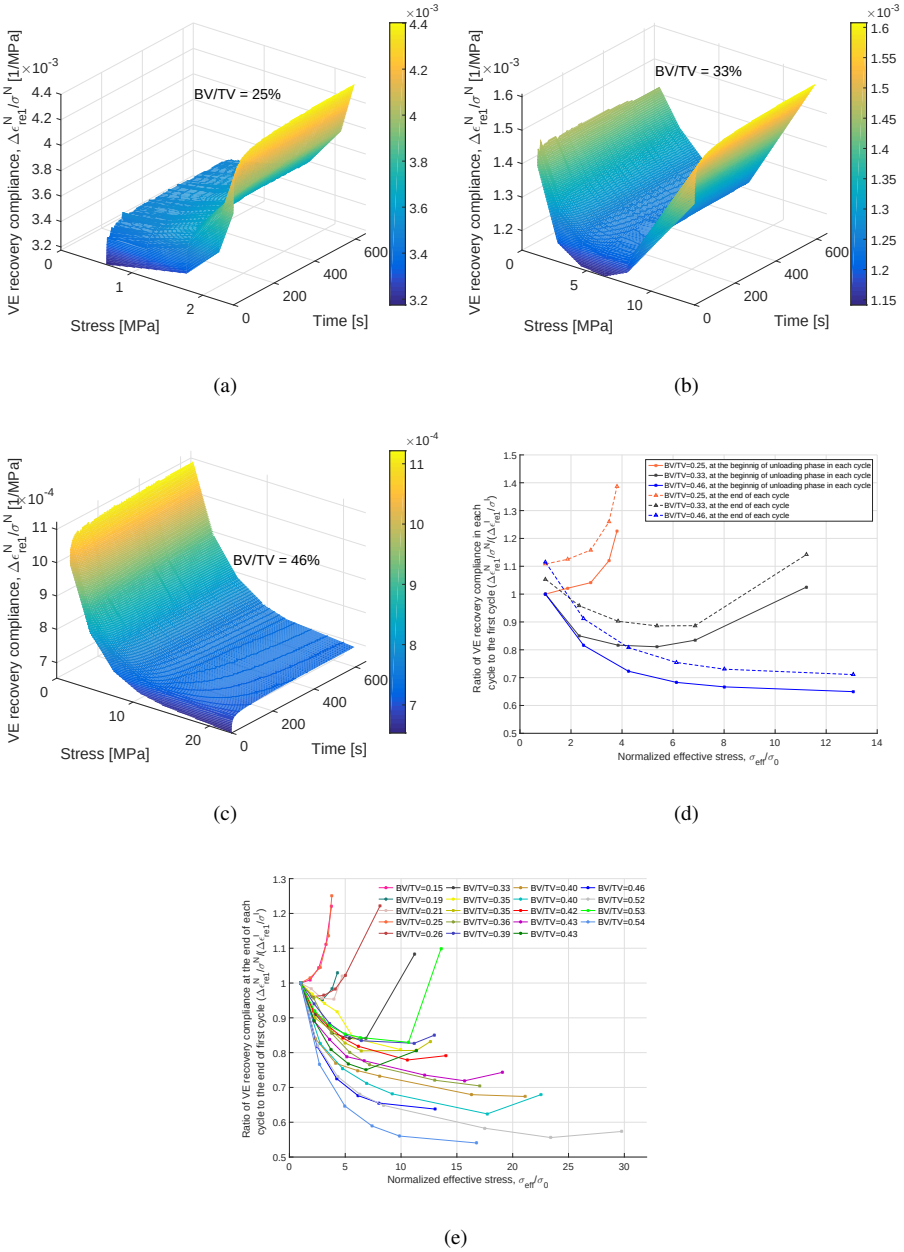

Fig. 4 Experimental viscoelastic recovery compliance with the time and stress for samples: (a) S25 (BV/TV = 0.25), (b) S33 (BV/TV = 0.33), and (c) S46 (BV/TV = 0.46); (d) the ratio between the viscoelastic recovery compliance and the respective instantaneous compliance for each of the three samples plotted plotted against normalized effective stress, and (e) the ratio of viscoelastic recovery compliance at the end of each cycle to the respective value at the end of first cycle plotted against normalized effective stress for all 19 samples. Purely recoverable response was obtained from $\Delta\varepsilon_{re1}^{N}$ in each loading cycle.

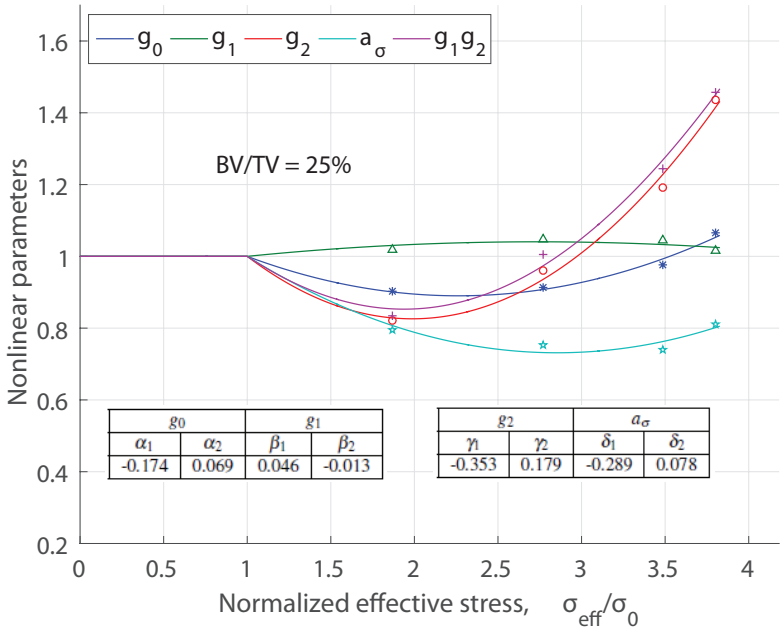

g_0		g_1	
α_1	α_2	β_1	β_2
-0.174	0.069	0.046	-0.013

g_2		a_σ	
γ_1	γ_2	δ_1	δ_2
-0.353	0.179	-0.289	0.078

(a)

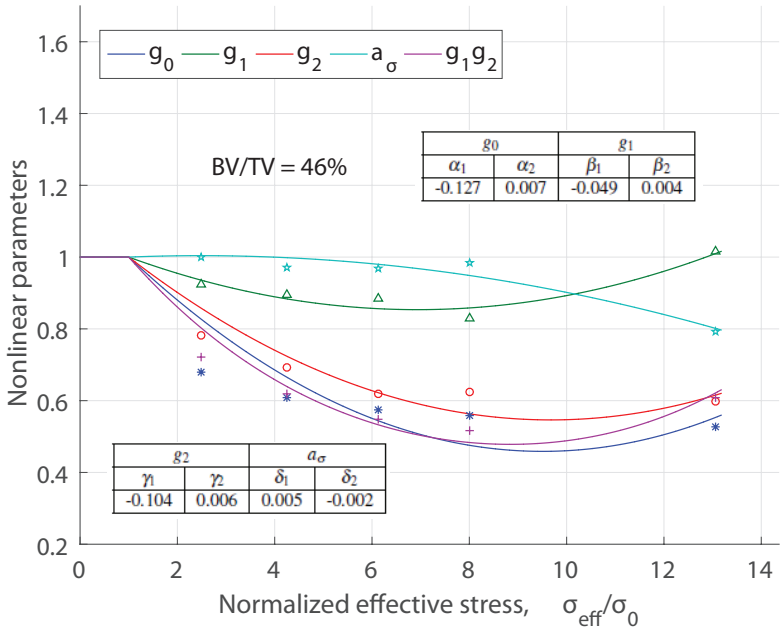

g_0		g_1	
α_1	α_2	β_1	β_2
-0.127	0.007	-0.049	0.004

g_2		a_σ	
γ_1	γ_2	δ_1	δ_2
-0.104	0.006	0.005	-0.002

(b)

Fig. 5 Nonlinear viscoelastic parameters, g_0, g_1, g_2 and a_σ, expressed as second order polynomial functions of effective stress (Eqs. 19 - 22) are plotted against normalized effective stress for two samples with (a) BV/TV = 0.25 and (b) BV/TV = 0.46.

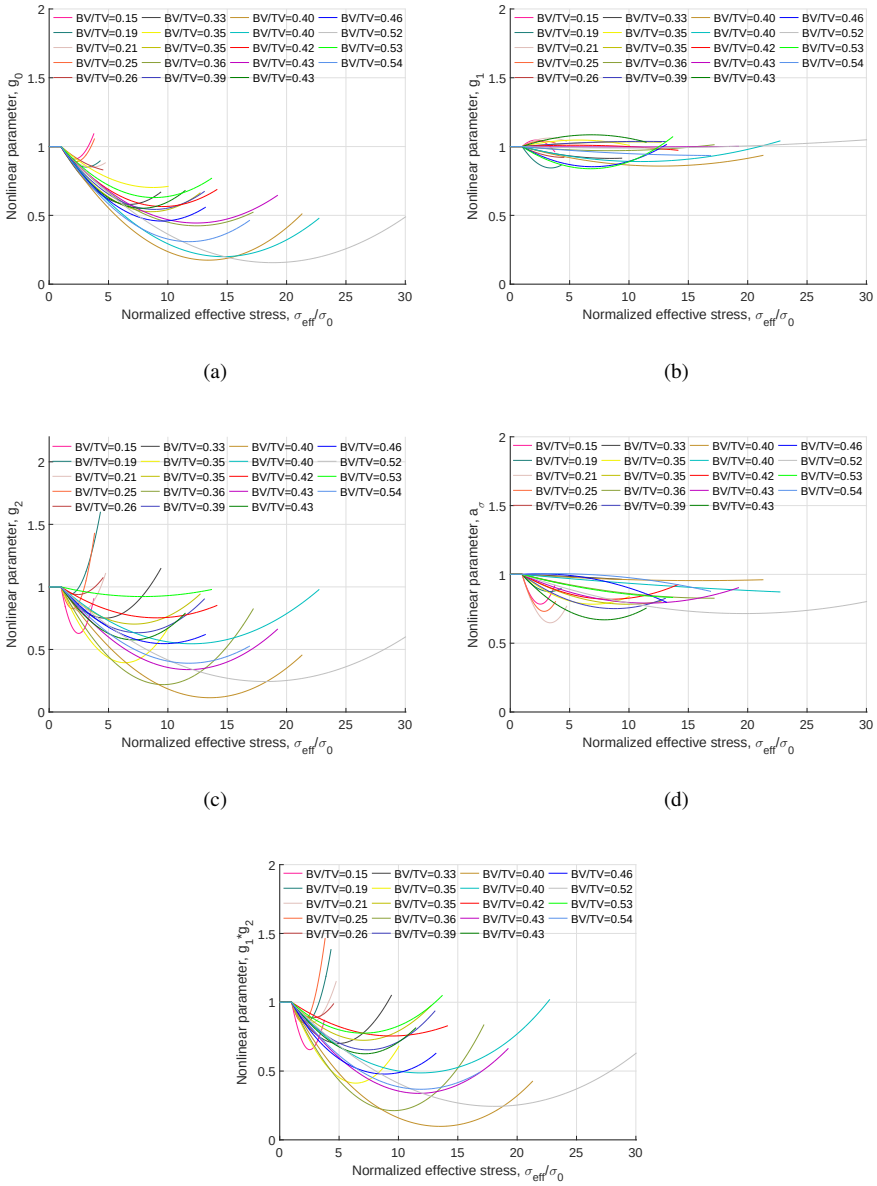

Fig. 6 Nonlinear VE parameters, expressed as second order polynomial functions of effective stress, for all 19 samples are plotted against normalized stress, (a) parameter g_0, (b) parameter g_1,(c) parameter g_2, (d) parameter a_σ, and (e) product of th parameters g_1 and g_2.

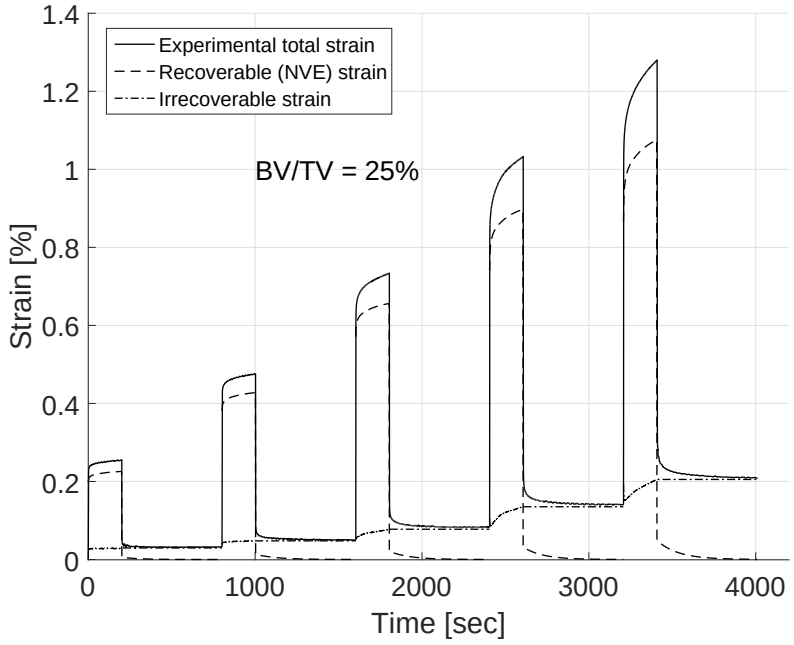

(a)

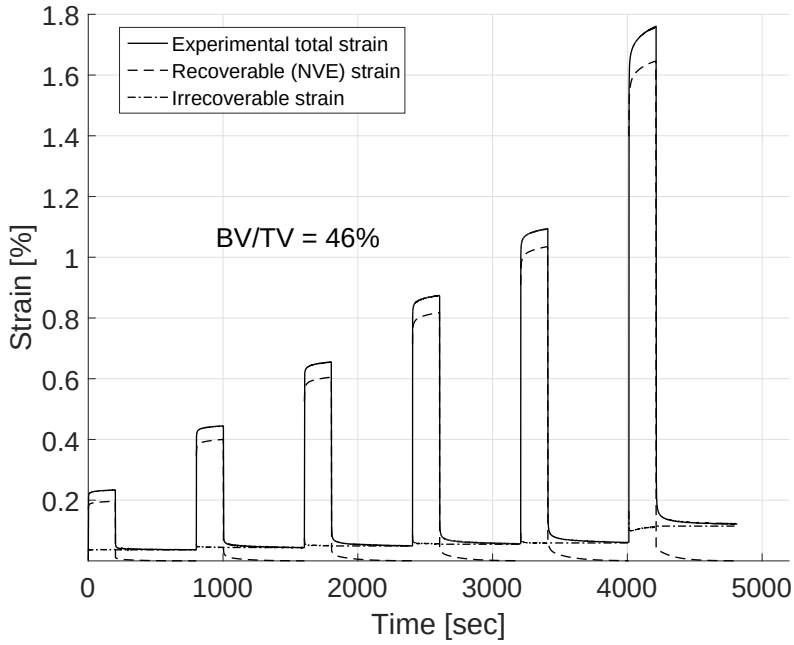

(b)

Fig. 7 The pure viscoelastic and the irrecoverable strain responses are plotted along with the total creep strain response for two typical samples S25 and S46, (a) BV/TV = 0.25 and (b) BV/TV = 0.46, respectively.

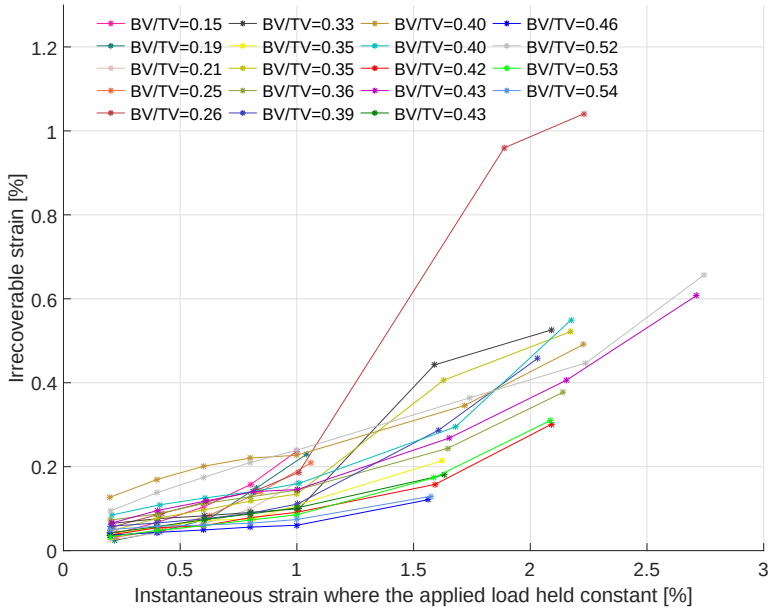

(a)

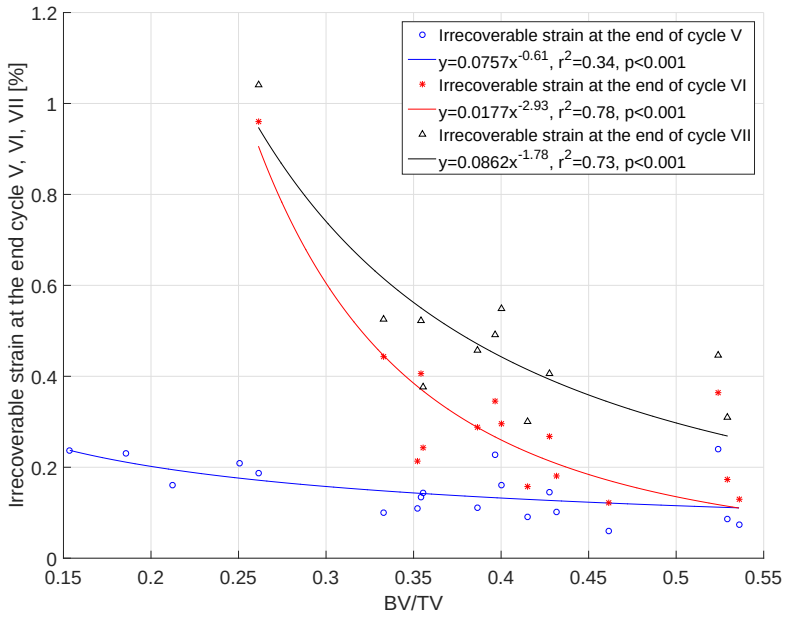

(b)

Fig. 8 (a) Irrecoverable strains at the end of each loading cycle in each sample with the applied static strain (where plateau force was held constant during creep-recovery test), (b) irrecoverable strains in cycle V, VI, VII corresponding to static strains of 1.0%, 1.5% and 2.0% are plotted against BV/TV of all samples.